J Mater Sci (2010) 45:1809–1816
DOI 10.1007/s10853-009-4163-7

Dislocation evolution in interstitial-free steel during constant and variable amplitude testing

Chia-Chang Shih · New-Jin Ho · Hsing-Lu Huang

Received: 22 January 2009 / Accepted: 23 December 2009 / Published online: 20 January 2010

Abstract This study aimed to understand the relationship between gliding behavior of dislocations and reversed evolution of dislocation structures in pure body-centered cubic metals, using automotive-grade interstitial-free steels under strain ratio = 0 for case studies. Dislocation cells were converted into loop-patch structures, and the gilding behavior of dislocations would have changed from the original multiple-slips to single-slip when the maximum strain was reduced from 1.2 to 0.15 or 0.2%. The extent to which the reversed evolution of dislocation structures occurs is lower for maximum strain = 0.15% as compared to that of maximum strain = 0.2%. However, once the maximum strain is reduced to 0.1%, dislocation cells would persist, showing no signs of reversed evolution. A strain threshold for reversed evolution of dislocation structures was inferred to fall between maximum strain = 0.1% and maximum strain = 0.15%.

Introduction

The development of dislocation structures in cyclically deformed coppers has been quite thoroughly studied. It is accepted that the dislocation evolution in low-cycle fatigue for most metals at low strain amplitudes is a step-by-step process. For example, the sequence of dislocation structure evolution for a fatigued polycrystalline copper goes by loop patches, veins structure, persistent slip bands (PSBs, or called dipolar wall), dislocation walls, and dislocation cells [1–8]. In two-step test, Ma and Laird [9] demonstrated that dislocation cells developed at higher strain amplitudes, because multiple slips could reversibly transform back to loop patches. Recently, similar reversed transformation of dislocation cells has also been reported by Huang [10]. He indicated that the cells and dipolar walls would transform back to loop patches when the strain amplitude was decreased from 0.3 to 0.1% in low-cycle fatigue. Therefore, reversed evolution of dislocation structures in cyclically deformed coppers is a proven phenomenon after a two-step fatigue experiment.

Compared with fatigued coppers, studies in the past decades on the sequence of formation for dislocation structures of fatigued body-centered cubic (BBC) metals are very limited [11–15], not to mention the high–low strain-controlled fatigue tests. So far, only Chopra and Gowda [16] have investigated on the alpha iron decades ago but found no reversed development of dislocation structures. Therefore, the understanding of reversed development of dislocation structures in BCC metals remains incomplete. The purpose of this study is to clarify whether the reversed evolution of dislocation structures observed in fatigued coppers also occurs in pure BCC metals. We employ transmission electron microscopy (TEM) and scanning electron microscopy (SEM) to analyze the influences of various strain amplitudes before and after the two-step fatigue experiments.

Experimental

Cylindrical specimens of 8 mm in diameter and 15 mm in gauge length were prepared from a 15-mm thick hot-rolled

C.-C. Shih · N.-J. Ho
Institute of Materials Science and Engineering, National Sun Yat-Sen University, Kaohsiung, Taiwan, ROC

H.-L. Huang (✉)
Department of Mechanical Engineering, Chinese Military Academy, Kaohsiung, Taiwan, ROC
e-mail: hlhuang8423@gmail.com

interstitial-free steel (IF steel) polycrystalline plate with a chemical composition of C < 50 ppm, N < 50 ppm, S < 120 ppm, B ≈ 2 ppm, Mn ≈ 0.15 wt%, Ti ≈ 0.04 wt%, and balanced Fe. The steel blocks were annealed at 800 °C for 2 h and then cooled in furnace to obtain an averaged grain size of 80 μm. The preparation of specimen followed the ASTM E606 specification. Constant-strain and two-step fatigue tests were conducted at room temperature in a computerized Instron 8801 hydraulic testing machine at a strain rate of 4×10^{-3} s^{-1}. The constant-strain fatigue tests were performed with maximum strain (ε_{max}) of 0.1, 0.15, 0.2, and 1.2%, and 2×10^6, 1×10^5, 3000, and 30 cycles for sample A, B, C, and D, respectively, all under strain ratio (R) = 0 condition. For two-step fatigue tests, the samples were first cycled at $\varepsilon_{max} = 1.2\%$ for 30 cycles and then to 1×10^5, 1×10^5, and 3000 cycles with the maximal strain reduced to 0.1% (sample E), 0.15% (sample F), and 0.2% (sample G), respectively. The fatigue test data for all samples are summarized in Table 1. All fatigued samples were cut into slices of 1 mm thickness in cross sections. The slices were ground to a thickness of about 0.3 mm for SEM and 0.1 mm for TEM observations using abrasive paper and punched into discs of 3-mm in diameter. The 3-mm discs were twin-jet polished using a solution of 90% methanol diluted with 10% perchlorate at 15 V and −40 °C. For microstructure observations, a Philips Quant200 SEM under backscattered electron imaging (BEI) mode was used to obtain electron channeling contrast images (ECCI), and a Philips CM200 TEM under bright-field imaging (BFI) mode where the two-beam mode was employed to obtain images of higher resolution for comparison with the SEM images.

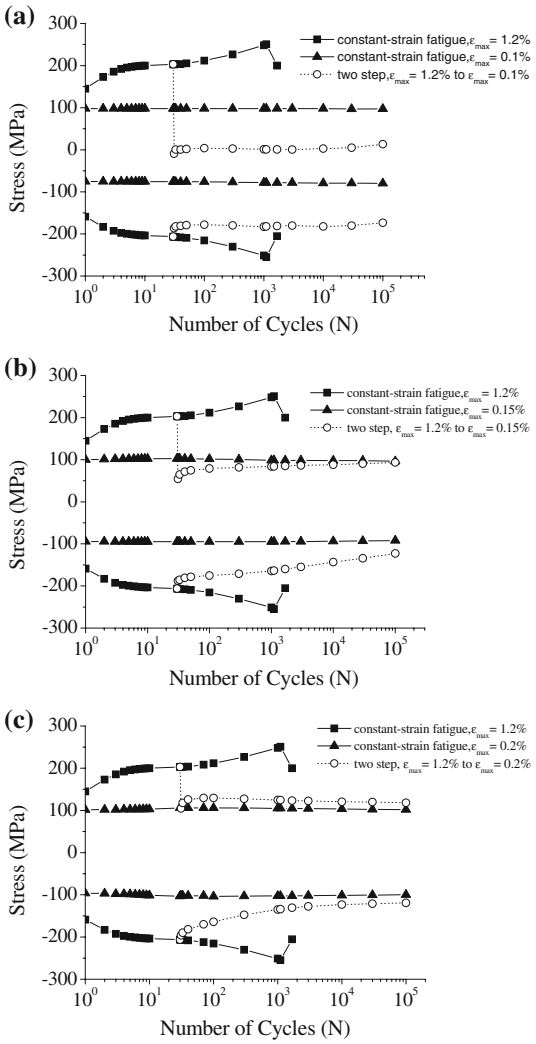

Fig. 1 Cyclic stress responses with the number of cycles were plotted at various two-step strain fatigue tests: **a** $\varepsilon_{max} = 1.2$ to 0.1% (sample E); **b** $\varepsilon_{max} = 1.2$ to 0.15% (sample F); and **c** $\varepsilon_{max} = 1.2$ to 0.2% (sample G)

Results and discussion

The cyclic responding stresses versus the number of cycles (S–N curve) for the tested specimens are shown in Fig. 1, while all the test results are summarized in Table 1. For the constant-strain test under a maximal strain of 1.2% (sample D), the rapid hardening, which occurred during the early stage of cycling, and the secondary hardening stage prior to failure have also been reported by Chopra and Gowda [16] for the alpha iron. As for the cycling at $\varepsilon_{max} = 0.1$, 0.15,

Table 1 The fatigue test data at different strain amplitude

Sample	Maximum strain (%)	Reduce maximum strain (%)	Reduce after cycle	Number of cycles after reducing maximum strain	Final cycle
A	0.1	No	–	–	2×10^6
B	0.15	No	–	–	1×10^5
C	0.2	No	–	–	3000
D	1.2	No	–	–	30
E	1.2	0.1	30	1×10^5	100030
F	1.2	0.15	30	1×10^5	100030
G	1.2	0.2	30	3000	3030

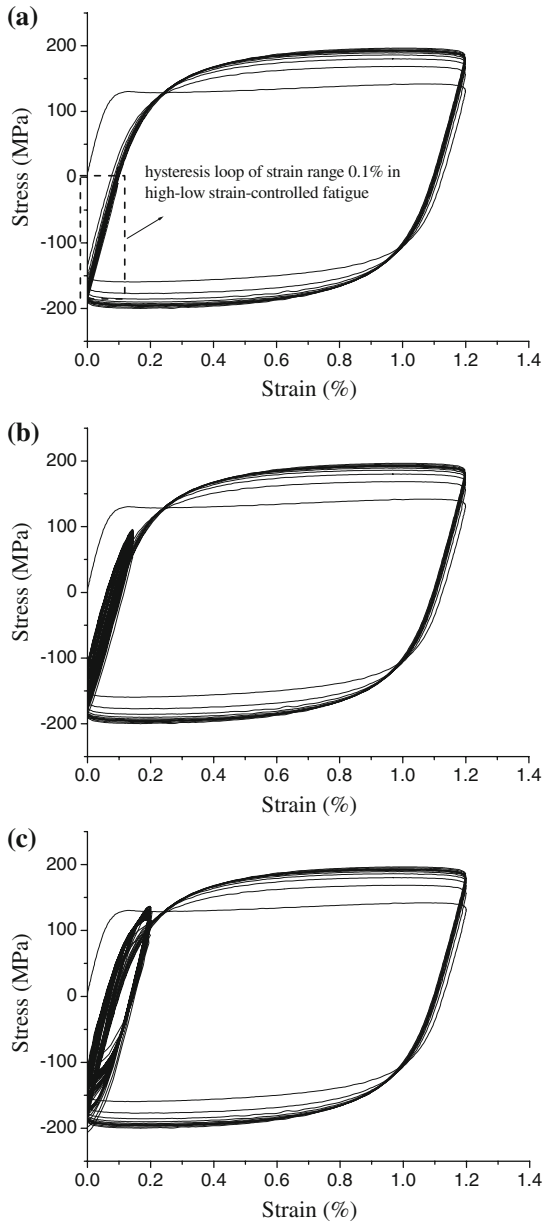

Fig. 2 Hysteresis loops for various two-step fatigue tests: **a** ε_{max} = 1.2 to 0.1%; **b** ε_{max} = 1.2 to 0.15%; and **c** ε_{max} = 1.2 to 0.2%

and 0.2% (sample A, B, and C), the cyclic hardening is not obvious. For the two-step test, the stresses were followed by a decrease of ε_{max} from 1.2 to 0.1, 0.15, and 0.2% for sample E, F, and G, respectively. Sample E reveals no evidence of cyclic hardening or softening because the stress range was constant. Samples F and G exhibit cyclic softening, with the extent of cyclic softening for sample G being higher than that of the sample F. Figure 2a–c compares hysteresis loop for samples E, F, and G. The stresses and area of hysteresis loops all were reduced when the maximal strains were decreased. The area of the hysteresis loop for $\varepsilon_{max} = 0.1\%$ is too small to be distinguished from that of $\varepsilon_{max} = 1.2\%$.

In order to compare the two-step processes, it is necessary to examine the dislocation structures originated from samples A, B, C, and D with the SEM and TEM. Figure 3a shows sample A is nearly dislocation free after 2×10^6 cycles at $\varepsilon_{max} = 0.1\%$ as seen from the SEM/ECCI mode; this implies that almost no dislocation arrangements can be found in sample A. Figure 3b shows the detailed TEM examination, where only some gliding primary screw dislocations and a few debris loops can be found. For sample B (cycled to 1×10^5 cycles at $\varepsilon_{max} = 0.15\%$), as shown in Fig. 4a (SEM micrograph) and b (TEM micrograph), loop-patch structure is the only structure which can be observed. As for sample C (cycled to 3000 cycles at $\varepsilon_{max} = 0.2\%$) shown in Fig. 5a (SEM micrograph), loop-patch structure is also the only structure which can be seen. Figure 5b–d shows the similar effect for the TEM counterparts, where the contrast of loop patches has reduced significantly when $g = [10\text{-}1]$ at $B \approx [111]$. Hence, the dislocations that form these loop patches are mainly composed of the primary Burgers vector (bp) of [1–11]. By comparison, sample D ($\varepsilon_{max} = 1.2\%$ and cycled to 30 cycles) shown in Fig. 6a (SEM micrograph) and b (TEM micrograph) exhibits only dislocation-cell structure which can be found after cyclic deformation. Therefore, gliding behavior of dislocations in sample D is multiple slips. Figure 7a and b shows the corresponding dislocation

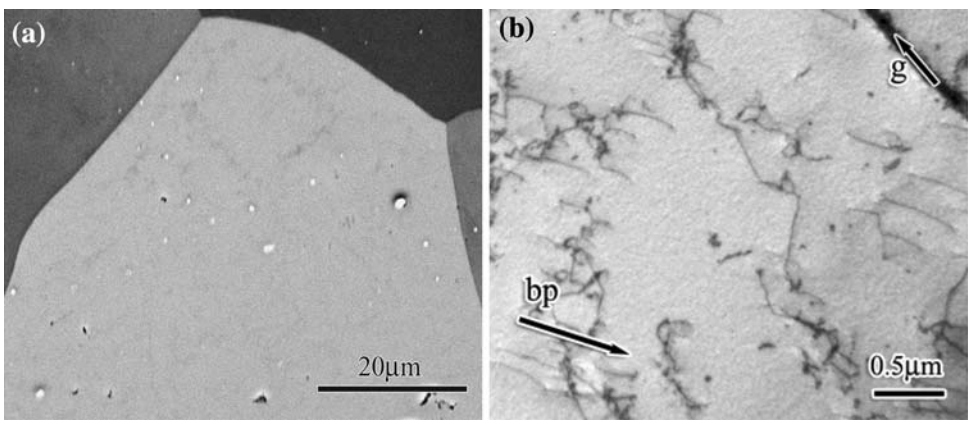

Fig. 3 Microstructure of IF steel cyclically deformed at $\varepsilon_{max} = 0.1\%$ and cycled to 2×10^6 cycles (sample A): **a** SEM-ECCI micrograph; and **b** TEM micrograph

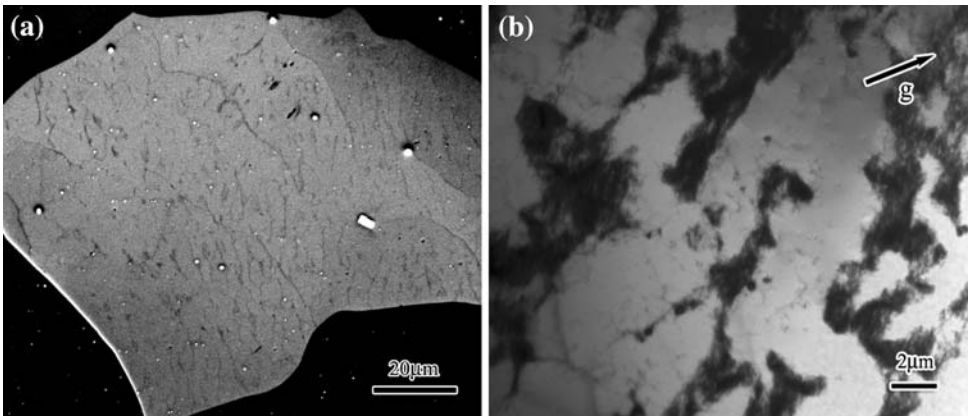

Fig. 4 Microstructure of IF steel cyclically deformed at $\varepsilon_{max} = 0.15\%$ and cycled to 1×10^5 cycles (sample B): **a** SEM-ECCI micrograph showing that the grain is filled with loop patches; and **b** TEM micrograph, where $B \approx [111]$, $g = [01-1]$

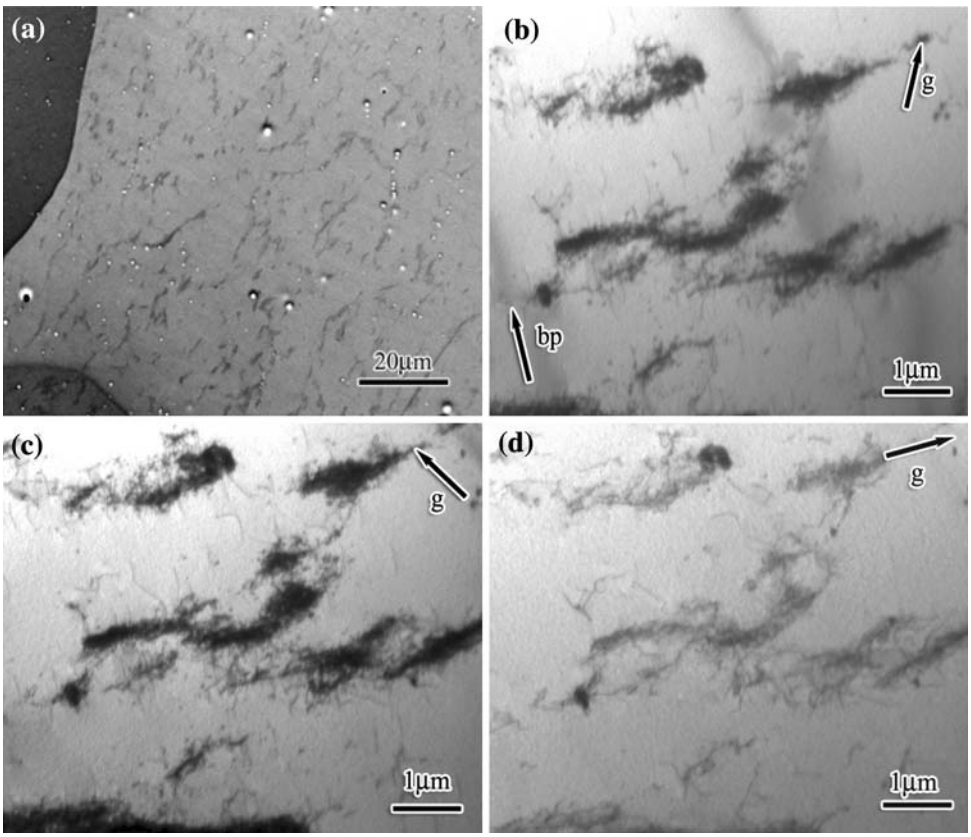

Fig. 5 Microstructure of IF steel cyclically deformed at $\varepsilon_{max} = 0.2\%$ and cycled to 3000 cycles (sample C): **a** SEM-ECCI micrograph showing that the grain is filled with loop patches; **b** TEM micrograph, where $B \approx [111]$, $g = [01-1]$; **c** same as (**b**), where $B \approx [111]$, $g = [1-10]$, and **d** same as (**b**), where $B \approx [111]$, $g = [10-1]$

structures of sample E under SEM and TEM, respectively, where only dislocation-cell structure exists. These dislocation cells persist through the high–low strain-controlled fatigue tests. The corresponding dislocation structures of sample F under the SEM/ECCI mode are given in Fig. 8a, where only dislocation cells are seen in the grain, and in Fig. 8b, where both loop patches and dislocation cells can be seen in the identical grain, implying in some grains the dislocation cells have not been changed. The volume fraction of loop patches in sample F is about 10%. Figure 9a shows the TEM counterpart of Fig. 8b, clearly revealing the conversion of dislocation cells into loop patches. Figure 9b–d shows the detailed examination of the region marked W in Fig. 9a, where the contrast of loop patches has been reduced and the primary screw dislocations in the channels of the loop patches become invisible when $g = [10\text{-}1]$ at $B \approx [111]$, thus these loop patches and screw dislocations are mainly composed of the primary Burgers vector (bp) of [1–11]. For sample G (cycled to 3000 cycles after the strain was reduced from $\varepsilon_{max} = 1.2$ to 0.2%), however, the dislocation cells have been partially transformed into loop patches, as reflected in Fig. 10a and b where the SEM/ECCI images are shown. On a more detailed analysis, we find that almost all grains in sample

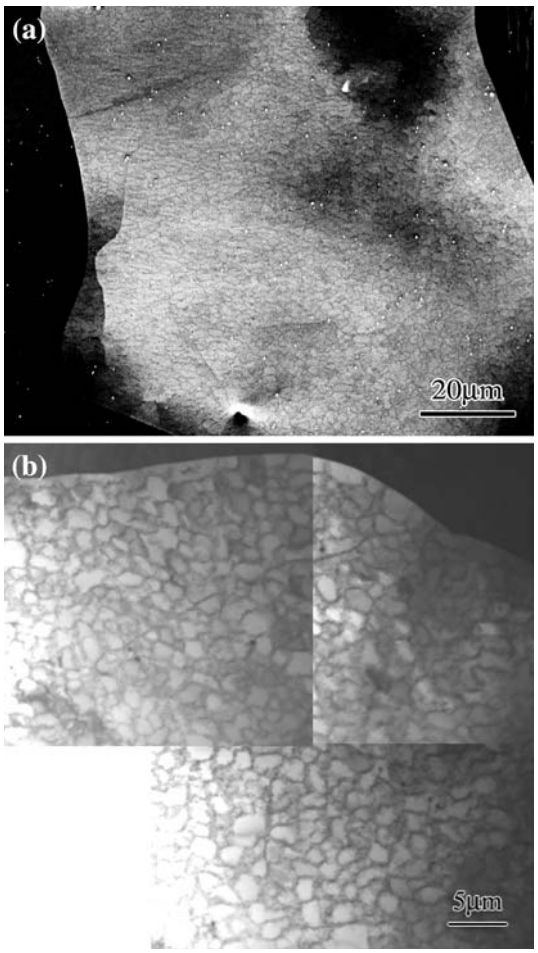

Fig. 6 Microstructure of IF steel cyclically deformed at $\varepsilon_{max} = 1.2\%$ and cycled to 30 cycles (sample D): **a** SEM-ECCI micrograph; and **b** TEM micrograph

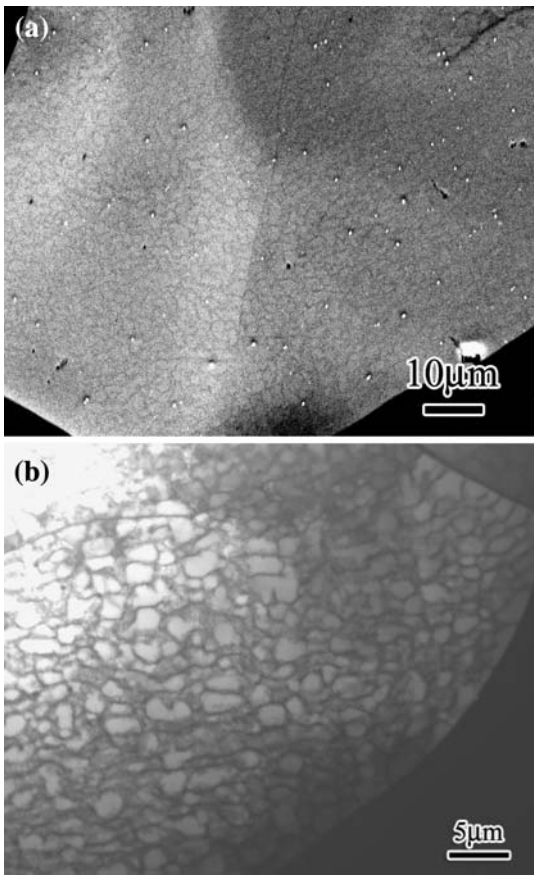

Fig. 7 Microstructure of IF steel cyclically deformed at 1×10^5 cycles after a decrease of strain amplitude from $\varepsilon_{max} = 1.2$ to 0.1% (sample E): **a** SEM-ECCI micrograph; and **b** TEM micrograph

G, the dislocation-cell structures, have been changed and the total volume fraction of loop patches in sample G is about 20%. The comparison morphology as examined more carefully by TEM is shown in Fig. 11a–d; Fig. 11b–d gives the details of the area marked R in Fig. 11a, where the loop patches and screw dislocations are, as usual, mainly composed of primary Burgers vector [1–11].

We now know almost no dislocation arrangement was found in sample A, and the loop patches in samples B and C are mainly composed of primary dislocations, thus the gliding of dislocations in samples B and C have occurred by single-slips principally. By comparison, sample D ($\varepsilon_{max} = 1.2\%$ and cycled to 30 cycles) exhibits only dislocation-cell structures. Therefore, the dislocation structures in sample D must have originated from multiple slips. However, loop-patch structure emerges after the ε_{max} was reduced from 1.2 to 0.15 and 0.2% (samples F and G), which implies that some dislocation cells for $\varepsilon_{max} = 1.2\%$ have been converted into loop patches, and simultaneously the gilding behavior of dislocations have changed from the original multiple-slips to single-slip. Nevertheless, no similar phenomenon was found in sample E (ε_{max} was reduced from 1.2 to 0.1%). Hence, we believe this has something to do with the gliding behavior of the dislocations. Since there is no loop-patch structure in sample D, unlike in samples F and G, we believe that the dislocation cells must have been converted into loop-patch structures after the high–low strain tests from $\varepsilon_{max} = 1.2$ to 0.2%. This new finding supplements the report by Chopra and Gowda [16]. Ma and Laird [9] had suggested that there is an equilibrium between dislocation multiplication and annihilation established in the dislocation cells while dislocation cells are formed. However, if the constant-strain amplitude is changed from high to low, the equilibrium between dislocation multiplication and annihilation may no longer exist. If the strain amplitude or applied stress is large enough to keep the dislocation sources active, but not large enough to drive these dislocations into adjacent walls and to force them to annihilate with the dislocations of opposite sign, then the processes of multiplication will exceed those of annihilation. This argument is consistent

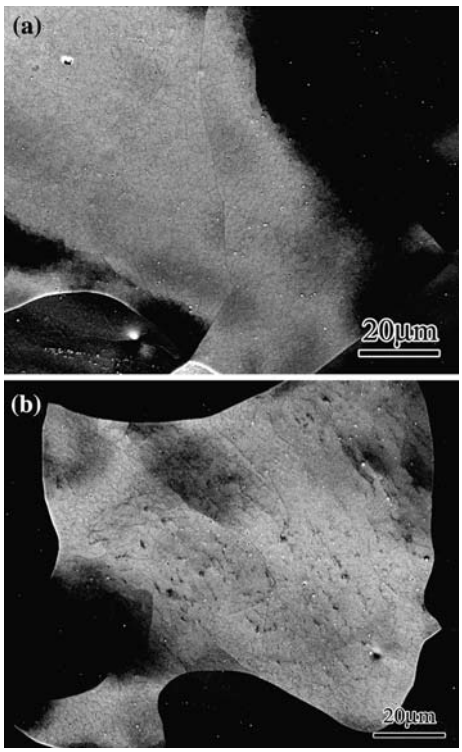

Fig. 8 SEM-ECCI micrographs of IF steel cyclically deformed at 1×10^5 cycles after a decrease of strain amplitude from $\varepsilon_{max} = 1.2$ to 0.15% (sample F): **a** this micrograph exhibits that the dislocation cells have not been changed; and **b** this micrograph exhibits that some loop patches can be found in the grain interior

with the observations from samples F and G in this study. The corresponding structures of $\varepsilon_{max} = 0.15$ and 0.2% (samples B and C) are loop patches of primary dislocations, and much like what was found in samples F and G. It is well known that the dislocations will be gathered to form the loop patches on the primary slip plane, while gliding behavior of dislocations is single slip [2, 17]. Therefore, we believe that once the strain amplitudes were decreased from $\varepsilon_{max} = 1.2$ to 0.15 and 0.2%, the multiple-slip processes will change into single-slip ones whence the dislocation density will increase, thus making the equilibrium between dislocation multiplication and annihilation established in the dislocation cells unsustainable. That is to say, the multiplications will exceed annihilation of the dislocations, and this is the main reason why the dislocation cells were gradually transformed back into loop patches.

On the other extreme, the formation of loop patches and changes of dislocation structures have not been found in sample E. As indeed suggested by Ma and Laird [9], once dislocation multiplication exceeds annihilation established in the dislocation cells, the dislocation cells will be converted into loop patches. Since almost no dislocation arrangement has been found in sample A, thus the stress corresponds to 0.1% is too low to trigger the dislocation multiplications. This further implies that the dislocation multiplications may not take place as the maximum strain decreases from 1.2 to 0.1%. Therefore, in the case of

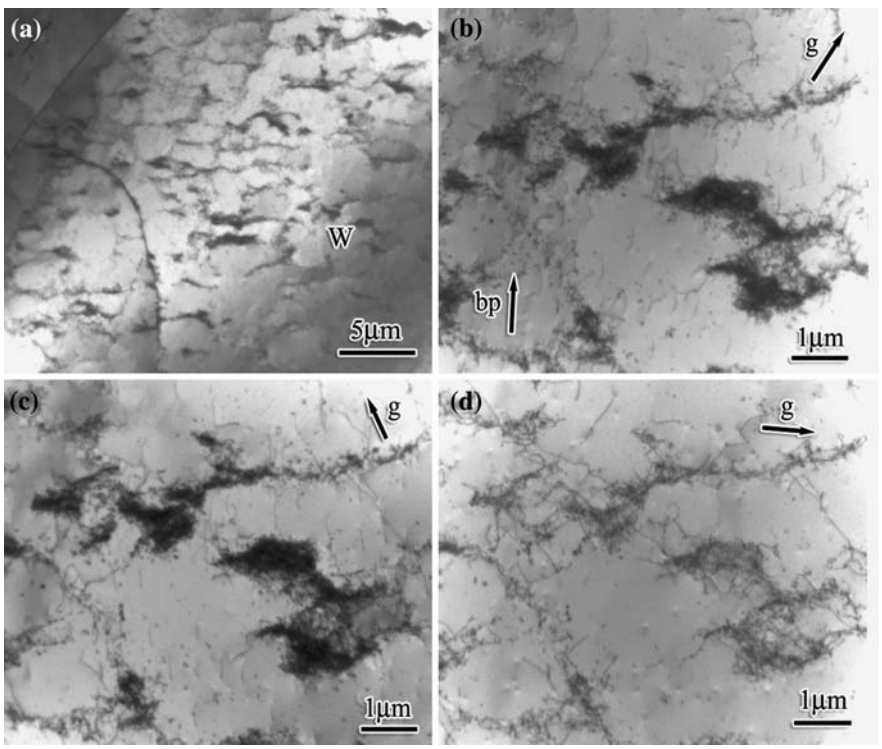

Fig. 9 TEM-micrograph observations of IF steel cyclically deformed at 1×10^5 cycles after a decrease of strain amplitude from $\varepsilon_{max} = 1.2$ to 0.15% (sample F): **a** low-magnification examination, where dislocation cells are gradually converted into loop patches; **b** mark W in **a** showing the detailed loop-patch structure, where $B \approx [111]$, $g = [01-1]$; **c** same as **b**, where $B \approx [111]$, $g = [1-10]$; and **d** same as **b**, where $B \approx [111]$, $g = [10-1]$

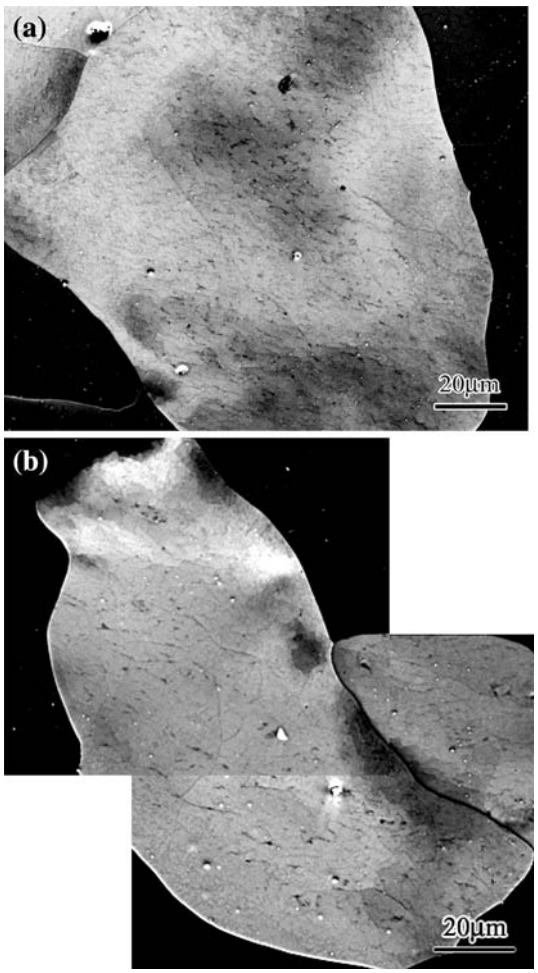

Fig. 10 SEM-ECCI micrographs of IF steel cyclically deformed at 3000 cycles after a decrease of strain amplitude from $\varepsilon_{max} = 1.2$ to 0.2% (sample G): **a** and **b** both exhibit that the dislocation cells were converted into loop patches to some extent

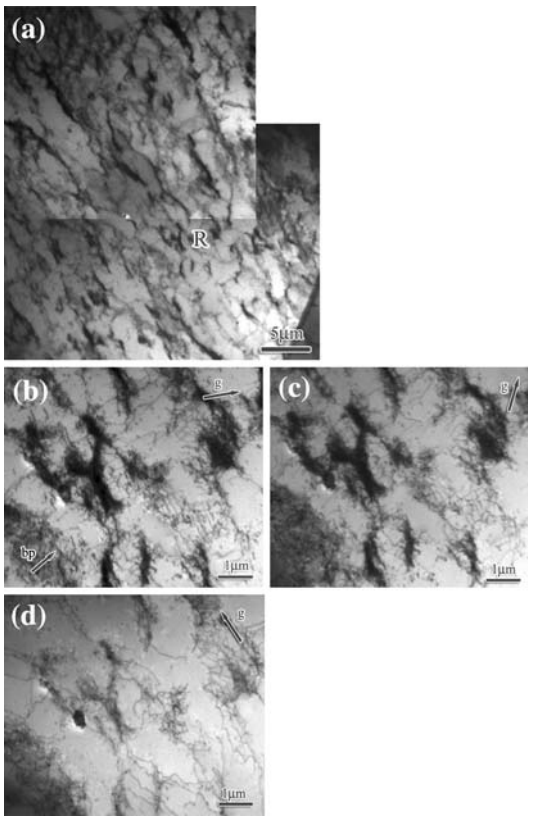

Fig. 11 TEM-micrograph observations of IF steel cyclically deformed at 3000 cycles after a decrease of strain amplitude from $\varepsilon_{max} = 1.2$ to 0.2% (sample G): **a** low-magnification examination, where dislocation cells are gradually converted into loop patches; **b** mark R in **a** showing the detailed loop-patch structure, where $B \approx [111]$, $g = [01-1]$; **c** same as **b**, where $B \approx [111]$, $g = [1-10]$; and **d** same as **b**, where $B \approx [111]$, $g = [10-1]$

sample E, the equilibrium between dislocation multiplication and annihilation established in the dislocation cells has still been maintained and still keep the original morphology. Among samples E, F, and G, only the sample E does not reveal cyclic softening, and the extent of softening of sample higher for sample G as compared to sample F. As the dislocations gliding between loop patches is easier than that inside dislocation cells, the cause of cyclic softening for samples F and G can be attributed to the formation of loop patches. The volume fraction of loop patches for samples F and G are about 10 and 20%, respectively, and this may well explain why the degree of cyclic softening in sample G is higher. Since the cyclic stresses corresponding to $\varepsilon_{max} = 0.15\%$ are lower than those for $\varepsilon_{max} = 0.2\%$, the gliding speed of dislocations and the extent of dislocation multiplication would also be lower. Therefore, the extent of the reversed evolution in sample F is inevitably lower than that in sample G. In short, a strain threshold for reversed evolution of dislocation structures in cyclically deformed IF steels should fall between $\varepsilon_{max} = 0.1$ and 0.15%.

Conclusion

1. Almost no dislocation arrangement can be found when the strain amplitude is controlled at $\varepsilon_{max} = 0.1\%$ and cycled to 2×10^{6} cycles (sample A). The corresponding structures in samples B ($\varepsilon_{max} = 0.15\%$ and cycled to 1×10^{5} cycles) and C ($\varepsilon_{max} = 0.2\%$ and cycled to 3000 cycles) are both of loop patches mainly composed of primary dislocations. Sample D ($\varepsilon_{max} = 1.2\%$ and cycled to 30 cycles) exhibits only dislocation-cell structures.
2. Dislocation cells were converted into loop patches, while ε_{max} was reduced from 1.2 to 0.15 and 0.2% (samples F and G), where the volume fraction of loop-patch structure was about 10% for sample F and 20% for sample G. However, once ε_{max} was reduced to 0.1% (sample E), dislocation cells show no changes.

3. The extent to which the dislocation cells were converted into loop patches in sample F was smaller than that in sample G, and no dislocation cells were changed in sample E. A strain threshold for reversed evolution of dislocation structures in cyclically deformed IF steels should fall between $\varepsilon_{max} = 0.1$ and 0.15%.

Acknowledgements This research was supported by the National Science Council, Taiwan, ROC, under contract NSC94-2216-E-110-008, and partly by the Center for Nanoscience and Nanotechnology at NSYSU.

References

1. Kuhlmann-Wilsdorf D, Laird C (1980) Mater Sci Eng 46:209
2. Kuhlmann-Wilsdorf D, Laird C (1979) Mater Sci Eng 39:127
3. Kuhlmann-Wilsdorf D, Laird C (1977) Mater Sci Eng 27:137
4. Kuhlmann-Wilsdorf D, Laird C (1977) Mater Sci Eng 37:111
5. Kuhlmann-Wilsdorf D, Laird C (1977) Mater Sci Eng 39:231
6. Toribio J, Kharin V (2006) J Mater Sci 41:6015. doi:10.1007/s10853-006-0364-5-3
7. Chen CY, Huang JY, Yeh JJ (2003) J Mater Sci 38:817. doi:10.1007/s10853-006-0364-5-8
8. Laird C, Charsley P, Mughrabi H (1986) Mater Sci Eng 81:433
9. Ma BT, Laird C (1988) Mater Sci Eng A102:247
10. Huang HL (2003) Mater Sci Eng A342:38
11. Mughrabi H, Herz K, Stark X (1981) Int J Fract 17:193
12. Sommer C, Mughrabi H, Lochner D (1988) Acta Mater 46:1527
13. Šesták B, Novák V, Libovický S (1988) Philos Mag A57:353
14. Niendorf T, Canadinc D, Maier HJ, Karaman I (2008) Int J Fatigue 30:426
15. Mughrabi H, Herz K, Stark X (1976) Acta Metall 24:659
16. Chopra OK, Gowda CVB (1974) Philos Mag 30:583
17. Woods PJ (1973) Philos Mag 28:155